

# Semantic Richness or Geometric Reasoning? The Fragility of VLM’s Visual Invariance

Jason Qiu<sup>1\*</sup> Zachary Meurer<sup>1\*</sup> Xavier Thomas<sup>1\*†</sup> Deepti Ghadiyaram<sup>1,2</sup>

<sup>1</sup>Boston University <sup>2</sup>Runway

{jasonq, zmeurer, xthomas, dghadiya}@bu.edu

\*Equal contribution. †Corresponding author.

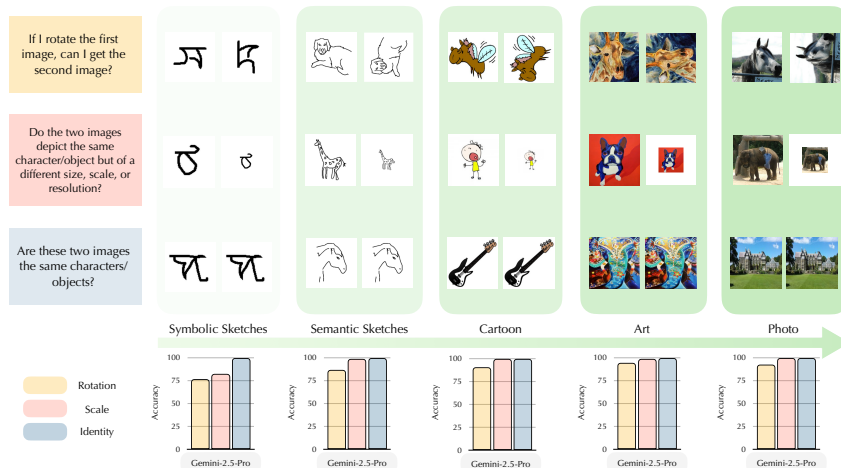


Figure 1: **Failure of visual transformation reasoning across visual domains.** Given a pair of images, models are asked to determine whether they depict the same object under transformations of rotation, scale, or identity. While performance remains near-perfect on natural images (Art, Photo), accuracy drops sharply on abstract and symbolic images (Symbolic and Semantic Sketches), particularly for rotation. Results shown are for Gemini-2.5-Pro (Comanici et al., 2025), with similar trends across evaluated MLLMs.

## Abstract

This work investigates the fundamental fragility of state-of-the-art Vision-Language Models (VLMs) under basic geometric transformations. While modern VLMs excel at semantic tasks such as recognizing objects in canonical orientations and describing complex scenes, they exhibit systematic failures at a more fundamental level: lack of robust spatial invariance and equivariance required to reliably determine object identity under simple rotations, scaling, and identity transformations. We demonstrate this limitation through a systematic evaluation across diverse visual domains, including symbolic sketches, natural photographs, and abstract art. Performance drops sharply as semantic content becomes sparse, and this behavior is observed across architectures, model capacities, and prompting strategies. Overall, our results reveal a systematic gap between semantic understanding and spatial reasoning in current VLMs, highlighting the need for stronger geometric grounding in future multimodal systems.

## 1 Introduction

Imagine being presented with a sentence in an unfamiliar script, such as *Glagolitic*. To identify repeating characters, we tend to rely solely on rigorous geometric analysis – matching curves, angles, and topology of characters. Now, consider performing the same task on your native script. The task becomes almost trivial due to semantic familiarity with the characters bypassing the need for shape reasoning. This human ability to fluidly switch between geometric reasoning and semantic recognition as needed raises a critical question: do present day vision-language models (VLMs) possess similar robustness?

To study this, we evaluate models across a spectrum of semantic granularity, ranging from sparse symbolic sketches and handwritten scripts to texture-rich photographs (Figure 1). Within these domains, we test three fundamental transformations: rotation, scaling, and identity matching. A VLM truly possessing geometric reasoning should identify if two images depict the same content regardless of the transformation applied. Crucially, this capability should remain consistent across both familiar (e.g., Latin) and unfamiliar (e.g., Glagolitic) scripts, semantic sketches, and real photos, as the underlying reasoning remains identical. If, however, a model’s apparent robustness is merely a byproduct of data familiarity or context, the performance should collapse on semantically sparser content.

Our in-depth analysis confirms this suspicion: the performance of even top-tier closed- and open-sourced VLMs collapses on semantically sparse content under basic geometric transformations. We demonstrate that the apparent invariance observed in real-world images is not just because of geometric reasoning, but rather a byproduct of dataset familiarity and prompt sensitivity. Specifically, models achieve higher accuracy when asked if two images contain the *same object* than when asked if one is a *rotated variant* of the other. This inherent reliance on object labels – without a corresponding grasp of the object’s underlying geometry – reveals a fundamental flaw in current VLMs. Given their pervasive deployment in safety-critical fields like robotics (Li et al., 2024), this inability to decouple semantic identity from geometric orientation poses a significant risk to reliable spatial interaction.

While prior research has documented VLM failures on high-level reasoning tasks such as visual analogical reasoning (Yiu et al., 2024), object instance orientation (Zhang et al., 2024), depth estimation (Hemmat et al., 2024), or spatial correspondence (Feng et al., 2025), we go beyond identifying failure modes. By using the gradient of semantic information (hand written digits, sketches, and cartoons) as a “stress test” for pure shape and geometric perception, we determine if VLMs rely on universal geometric principles or semantic familiarity. Our results reveal several critical gaps of VLMs, which we summarize below:

- All models are highly sensitive to **data familiarity** in the case of symbolic scripts. They exhibit high performance on familiar scripts such as *Latin* and substantially lower performance on less familiar scripts such as *Grantha*.
- All models **perform best on real photos**, remain relatively strong on cartoons, but **degrade sharply on sketches and symbolic scripts** (Fig. 1), where semantic cues are sparse. For instance, for Gemini-2.5-Pro (Comanici et al., 2025), accuracy drops from 92.67% on photos to 76.49% on symbolic sketches for the rotation task, and from 99.81% to 82.56% for the scale task (Fig. 1).
- Among the transformations studied, rotation is consistently the most challenging, with models exhibiting particularly low performance even when performance on identity and scale tasks is much stronger.
- The observed failures persist across model architectures, model capacities, and prompting strategies, suggesting that the limitation is fundamental rather than a consequence of model size or prompt design.

## 2 Related Work

**Visual Reasoning in VLMs.** The rapid advancement of vision-language models (VLMs) has prompted the question of whether these models exhibit true visual reasoning capabilities or primarily rely on learned statistical patterns. Prior work has explored the shortcomings of VLMs on seemingly simple visual reasoning tasks, including object counting and recognition (Campbell et al., 2025; Chandhok et al., 2025). These failures have been further studied using tasks grounded in cognitive research (Ramakrishnan et al., 2025; Campbell et al., 2025; Wüst et al., 2024), as well as benchmarks inspired by development psychology (Chen et al., 2026; Yiu et al., 2024). However, these studies primarily evaluate visual tasks in semantically rich settings (e.g., real world photos) and do not explicitly isolate if failure arises from limitations in visual reasoning or from reliance on semantic cues.

**Are VLMs Transformation Invariant?** Unlike Convolutional Neural Networks, which exhibit translational equivariance due to their architecture (Kondor & Trivedi, 2018), vision

transformers (ViTs) — the visual backbones of VLMs — do not have inherent transformation equivariance (Ding et al., 2023). Prior work suggests that ViTs may exhibit emergent invariance properties, particularly for rotation (Mason et al., 2026). However, such invariance does not necessarily translate to robust transformation reasoning, and VLMs fail at tasks that require visual invariance across a variety of settings (Chen et al., 2026; Yiu et al., 2024; Ramakrishnan et al., 2025; Niu et al., 2026). While such failures have been documented in prior benchmarks, we instead evaluate how VLMs perform on transformation tasks across varying levels of semantic richness, revealing where these failures persist.

**Evaluating Bias Across Visual Domains.** Prior work on visual reasoning in VLMs has primarily focused on natural images (Hemmat et al., 2024; Chandhok et al., 2025; Niu et al., 2026; Zhang et al., 2024) and does not systematically evaluate performance across diverse visual domains (e.g., photos, cartoons, sketches). When analyses have been performed across multiple domains, they typically focus on robustness to distribution shifts or stylistic variations (Mason et al., 2026; Gao et al., 2025; Vo et al., 2025), rather than isolating the role of semantic richness in shaping model behavior. In contrast, we evaluate VLM performance across a spectrum of semantic richness (Yu et al., 2022), which allows us to disentangle geometric reasoning from reliance on semantic cues and exposes failure modes that remain hidden when evaluation is restricted to natural images.

### 3 Studying VLM’s invariance equivariance dilemma

Given an image  $I$ , let  $T$  denote a set of transformation functions that map an image to a transformed version  $I'$ . In our study,  $T = \{t_{\text{rotation}}, t_{\text{scale}}, t_{\text{identity}}\}$ , and  $I' = t(I)$ , where  $t \in T$ . Transformation equivariance refers to a model’s ability to recognize that  $I$  and  $I'$  depict the same underlying content while also identifying the applied transformation  $t \in T$ . Since VLMs are trained on large-scale datasets of natural images (Liu et al., 2023), we hypothesize that their equivariance behavior may be influenced by learned data priors rather than consistent geometric reasoning. To evaluate this, we consider images with varying levels of semantic richness (Yu et al., 2022), ranging from sparse sketches to photographs and abstract art. Below, we describe our experimental framework and corresponding research questions for evaluating these capabilities across different models.

#### 3.1 Experimental setup

##### 3.1.1 Datasets

We conduct our experiments on datasets of diverse semantic richness detailed below.

- **Omniglot** (Lake et al., 2015) consists of handwritten characters from 50 diverse scripts, ranging from widely recognized scripts such as Latin and Greek, to rarer scripts such as Manipuri and Glagolitic. It comprises 1,623 distinct character classes in total, each containing multiple exemplar images rendered as black binary strokes on a uniform white background. We study Omniglot as a primary benchmark for two strategic reasons: **(a) Decouple spatial reasoning and script familiarity:** The dataset’s inclusion of both more prevalent (e.g., Greek) and rare (e.g., Tagalog) scripts allows us to study whether VLM performance is driven by true geometric reasoning or merely by data familiarity. **(b) Controlled Visual Stimuli:** Omniglot data is devoid of background noise, textures, and complex scenes, offering control over confounding variables and allowing us to study spatial reasoning in isolation.
- **Times New Roman** (Morison & Lardent, 1932) is a dataset of English alphabet characters rendered in the standard Times New Roman typeface, thus offering a single, consistent canonical appearance. This dataset: (a) mirrors the **extreme prevalence** of English typography in web-scale pretraining data, and (b) the **structural precision** of digital fonts removes stroke ambiguity and serves as a controlled baseline to isolate the model’s geometric reasoning capabilities.
- **Handwritten English** (Mann, 2024) characters and digits complement Omniglot. Unlike Times New Roman, this dataset exhibits stroke-level variation characteristic of handwriting, while retaining the familiarity of English characters and digits.

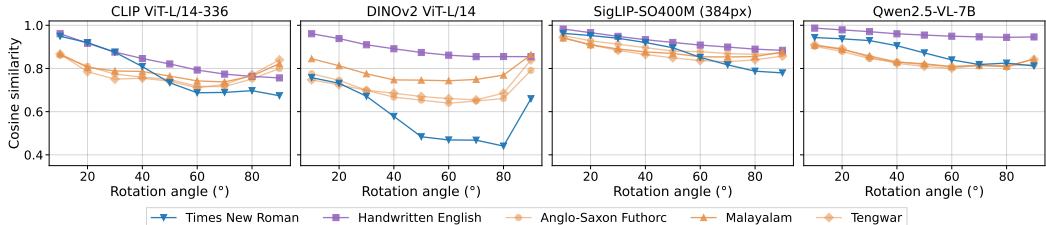


Figure 2: Cosine similarity between features extracted from different vision encoders on pairs of images under rotation. Select Omniglot scripts are shown in orange, while Times New Roman and Handwritten English are shown in blue and purple respectively. Across all encoders, similarity decreases with increasing rotation angle, with DINOv2 showing the steepest drop and SigLIP and Qwen2.5-VL-7B maintaining relatively higher similarity.

- **PACS** (Yu et al., 2022) dataset comprises 9,991 images of seven object categories (e.g., dog, guitar, elephant) spanning four visual domains: Photograph, Art Painting, Cartoon, and Sketch. Unlike the above character datasets, PACS offers high-level semantic content and exhibits substantial variation in texture, color, and level of visual abstraction. By evaluating models on this dataset, we can systematically analyze how geometric reasoning fluctuates for a single object category (e.g., dog) as its semantic representation becomes increasingly rich and complex.

Due to the high API costs of closed-source models, we sample a subset of each dataset for evaluation. For Omniglot, we sample one handwritten example from each character class across all 50 scripts, thereby evaluating on a total of 1,623 characters. For Handwritten English, we sample one handwritten exemplar per character, yielding 52 characters in total (both lower and upper-case characters). For Times New Roman, we evaluate on all 52 canonical characters from the English alphabet. For PACS (Yu et al., 2022) we randomly sample 200 images from each of the four domains, maintaining a balanced split across all 7 object categories within each domain, resulting in 800 images in total.

**Evaluation setup.** Each evaluation instance consists of a pair of images ( $I, I'$ ) and a text prompt (described later). The first image  $I$  is sampled from one of the above datasets. The second image  $I'$  is either (a) a **positive sample**,  $t(I)$  for  $t \in T$ , or (b) a **negative sample**,  $t(J)$ , a transformed version of a different image  $J$ . We prompt each model to determine if the two images depict the same underlying character or object under transformation  $t$ . For Handwritten English and Times New Roman, we avoid constructing negative pairs from upper and lower case variants of the same letter (e.g., 'a' and 'A'), as they correspond to the same underlying character and would make negatives ambiguous. A true positive (TP) corresponds to correctly identifying ( $I, t(I)$ ) as the same character or object, while a true negative (TN) corresponds to correctly identifying ( $I, t(J)$ ) as different. False positives (FP) and false negatives (FN) denote the respective misclassifications. We evaluate performance using the following metrics:

- **Recall (TPR).**  $TPR = TP / (TP + FN)$ .
- **Specificity (TNR).**  $TNR = TN / (TN + FP)$ .
- **Accuracy.**  $Accuracy = (TP + TN) / (TP + TN + FP + FN)$ .

**Models studied:** We study two powerful closed-sourced models: Gemini-2.5-Pro (Comanici et al., 2025) and GPT-5.2 (OpenAI, 2025), and two open-sourced models Qwen2.5-VL (Bai et al., 2025b), and Qwen3-VL (Bai et al., 2025a). Within the Qwen Series, we study different variants based on the number of parameters: Qwen2.5-VL-7B, Qwen2.5-VL-32B, Qwen3-VL-8B, Qwen3-VL-30B. Studying diverse models helps us understand the pervasiveness of current failures at various model capacities.

### 3.2 Studying transformation invariance in MLLMs

We use **rotation** as our main transformation to analyze the ability of Multi-Modal Large Language Models (MLLMs) to perceive transformations. Specifically, given two images, the task is to identify if the second one could be a rotated version of the first image. We study other transformations in Sec. 3.3.

Dataset	Qwen2.5-VL-7B			Qwen2.5-VL-32B			Qwen3-VL-8B			Qwen3-VL-30B			GPT-5.2			Gemini-2.5-Pro		
	Acc.	TNR	TPR	Acc.	TNR	TPR	Acc.	TNR	TPR	Acc.	TNR	TPR	Acc.	TNR	TPR	Acc.	TNR	TPR
Times New Roman	51.07	100.00	02.14	52.67	100.00	05.34	50.11	100.00	00.21	65.81	100.00	31.62	74.25	95.09	53.42	89.32	100.00	78.63
Handwritten English	50.85	98.08	03.63	62.50	98.08	26.92	50.00	100.00	00.00	55.98	100.00	11.97	67.84	96.58	39.10	68.27	99.57	36.97
Omniglot	50.72	99.46	01.98	54.17	94.71	13.62	51.01	99.96	02.06	56.64	99.75	13.53	75.55	80.91	70.19	76.90	98.69	55.10
Random guess	50.00	50.00	50.00	50.00	50.00	50.00	50.00	50.00	50.00	50.00	50.00	50.00	50.00	50.00	50.00	50.00	50.00	50.00

Table 1: **Rotation recognition performance across character datasets.** Best and worst accuracy per model across datasets are highlighted in teal and red, respectively. Performance is aggregated over rotation angles 10°–90°. While TNR remains near-perfect across all models, TPR is consistently low, indicating a failure to recognize rotated variants. Closed-source models perform better than open-source models, but the failure persists across all models.

Domain	Qwen2.5-VL-7B			Qwen2.5-VL-32B			Qwen3-VL-8B			Qwen3-VL-30B			GPT-5.2			Gemini-2.5-Pro		
	Acc.	TNR	TPR	Acc.	TNR	TPR	Acc.	TNR	TPR	Acc.	TNR	TPR	Acc.	TNR	TPR	Acc.	TNR	TPR
Photo	59.42	100.00	18.83	77.67	100.00	55.33	50.25	100.00	00.50	64.58	100.00	29.17	99.50	100.00	99.00	92.67	100.00	85.33
Art Painting	50.25	100.00	00.50	63.50	100.00	27.00	50.08	100.00	00.17	55.08	100.00	10.17	99.50	100.00	99.00	94.17	100.00	88.33
Cartoon	51.42	100.00	02.83	70.08	100.00	40.17	50.25	100.00	00.50	60.67	100.00	21.33	98.17	100.00	96.33	90.33	100.00	80.67
Sketch	52.25	100.00	04.50	57.25	100.00	14.50	50.42	100.00	00.83	52.83	100.00	05.67	92.25	99.67	84.83	86.50	99.83	73.17
Random guess	50.00	50.00	50.00	50.00	50.00	50.00	50.00	50.00	50.00	50.00	50.00	50.00	50.00	50.00	50.00	50.00	50.00	50.00

Table 2: **Rotation recognition performance across PACS domains.** Performance aggregated over rotation angles 90°, 180°, and 270°. While TNR remains near-perfect across models, TPR varies significantly across domains, with strong performance on photos and substantial degradation on sketches, indicating reliance on semantic cues rather than true geometric reasoning.

### 3.2.1 Are vision encoders rotational invariant?

To begin, we study how vision components within MLLMs behave under rotation. We compare vision encoders including CLIP ViT-L/14-336 (Radford et al., 2021), DINOv2 ViT-L/14 (Oquab et al., 2024), SigLIP-SO400M-384 (Zhai et al., 2023), and the visual encoder of Qwen2.5-VL-7B (Bai et al., 2025b) on the Omniglot dataset. For each encoder, we pass images through the pretrained backbone and extract a global image representation. We use the [CLS] token for CLIP and DINOv2, the multi-head attention pooling (MAP) output for SigLIP, and the mean of all image token features for Qwen2.5-VL-7B.

**Findings:** From Fig. 2, vision encoders exhibit high cosine similarity at smaller rotation angles (0°–30°), indicating that representations remain similar under minor transformations. As the rotation angle increases, similarity decreases across all encoders. DINOv2 shows the largest drop, particularly for Times New Roman, whereas SigLIP and Qwen2.5-VL-7B maintain relatively higher similarity at larger angles. English character sets (Times New Roman and Handwritten English) exhibit a more consistent monotonic decline with increasing rotation, while Omniglot scripts show non-monotonic trends. We next examine whether these feature similarities under rotation are sufficient for accurate transformation reasoning once coupled with a language decoder in MLLMs.

### 3.2.2 Are vision language models (VLMs) rotational invariant?

We use the data described in Sec. 3.1 to evaluate rotational invariance on 50 handwritten scripts from the Omniglot (Lake et al., 2015) dataset, along with the Handwritten English alphabet and the Times New Roman printed alphabet. We test on both positive and negative cases – i.e., where the two images are rotated versions of one another (ground truth response: “yes”) or where they are two different characters (ground truth response: “no”). We use the below prompt for the rotation invariance task, and test for 10°–90° rotations.

**Rotation Recognition Prompt** *If I rotate the first image, can I get the second image? Answer in curly brackets, e.g. {Yes} or {No}.*

**Findings:** Table 1 reports accuracy, TNR, and TPR across all datasets, with 50.00% corresponding to random guessing. Across all models, TNR remains high, while TPR is consistently low, indicating a strong bias toward predicting “{No}”. This results in near-random accuracy despite high TNR. For instance, Qwen2.5-VL-32B achieves a TPR of 5.34% on Times New Roman and 13.62% on Omniglot, while Qwen3-VL-30B reaches only 31.62% and 13.53%, respectively. Although closed-source models perform substantially better, even these models fail to achieve consistently high TPR across datasets: GPT-5.2 achieves a TPR of 53.42% on Times New Roman and 70.19% on Omniglot, while Gemini-2.5-Pro reaches 78.63% and 55.10%, respectively. Overall, these results indicate that identifying rotated variants of the same character remains a challenging task for current VLMs, reflecting a lack of robust geometric reasoning.

### 3.2.3 Suspect 1: Data bias

Models are trained primarily on natural images containing objects, complex scene structure, and textures (Liu et al., 2023). This raises the question: could it be that rotational invariance is domain-specific? To disentangle this, we replicate the study in Sec. 3.2.2 on PACS (Yu et al., 2022) using three rotations: 90°, 180°, and 270° across different visual domains (Fig. 4). These angles avoid *blank* padding pixels introduced by non-orthogonal rotations (e.g., 45°) (see suppl.). While this was not an issue for Omniglot (Lake et al., 2015) due to its uniform white background, such artifacts could otherwise confound performance on PACS images.

**Findings:** From Table 2, we observe almost no variation in TNR across models and domains, while TPR and accuracy vary substantially. Larger Qwen2.5-VL and Qwen3-VL models improve over their smaller counterparts, but remain significantly behind closed-source models such as GPT-5.2 and Gemini-2.5-Pro. Across all models, performance is highest on photos, followed by cartoons and art paintings, and consistently lowest on sketches. For example, Qwen2.5-VL-32B achieves a TPR of 55.33% on photos but only 14.50% on sketches, while Qwen3-VL-30B drops from 29.17% to 5.67% from photos to sketches. Even for closed-source models, this gap persists: GPT-5.2 achieves 99.00% TPR on photos but drops to 84.83% on sketches, and Gemini-2.5-Pro drops from 85.33% to 73.17%, respectively. Notably, closed-source models also exhibit a large drop when evaluated on symbolic sketches compared to semantic sketches. For instance, GPT-5.2 achieves a TPR of 84.83% on PACS sketches, but only 70.19% on Omniglot scripts (Table 1), indicating that performance degrades further as semantic richness decreases. This trend suggests that even strong models rely on semantic cues and data familiarity, and struggle when forced to operate purely on geometric structure.

### 3.2.4 Suspect 2: Model capacity

We study different variants from the family of Qwen2.5-VL and Qwen3-VL models and report the effect of model capacity on rotational invariance.

**Findings:** From Table 1, we observe a modest increase in accuracy with model capacity. For example, on Handwritten English, accuracy improves from 50.85% (Qwen2.5-VL-7B) to 62.50% (Qwen2.5-VL-32B), and on Times New Roman from 50.11% (Qwen3-VL-8B) to 65.81% (Qwen3-VL-30B). Similar trends are observed across datasets. However, TPR remains consistently low. Additionally, as reported in Table 2, while TPR is higher for Qwen2.5-VL-32B and Qwen3-VL-30B on real photos, with values of 55.33% and 29.17%, respectively, performance on sketches remains poor at 14.50% and 5.67%, indicating that scale alone is insufficient to improve robust geometric reasoning in VLMs.

### 3.2.5 Suspect 3: Brittleness to prompt

Next, we study whether the performance discrepancy between VLMs and visual encoders stems from *how* the task is phrased. Specifically, we wish to disentangle if a model’s understanding of rotation transformation is tied to its object recognition capability. On PACS dataset (Yu et al., 2022) (Sec. 3.1.1), we use the following prompts:

**Object Recognition focused (OR):** *Identify the main object in these images. Return ONLY the object name. Your options are: Dog, Elephant, Giraffe, Horse, Person, Guitar, or House.*

**Object Identification (OI):** *Is the object in these images a {class\_name}? Answer ONLY ‘Yes’ or ‘No’.*

**Rotation Recognition (RR):** *If I rotate the first image, can I get the second image? Answer in curly brackets, e.g. {Yes} or {No}.*

OR is formulated as a multi-class classification task without explicit negative samples, whereas OI and RR are binary tasks with both positive and negative samples (Sec. 3.1). The object categories used in the OR and OI prompts are from the PACS dataset. We hypothesize that object identification is a simpler task than recognition, enabling a more controlled assessment of VLM capabilities. Across all three tasks, we use images ( $I, I'$ ) as described for the rotation task ( $t_{\text{rotation}}$ ) in Sec. 3.1.1.

Domain	Qwen2.5-VL-7B			Qwen2.5-VL-32B			Qwen3-VL-8B			Qwen3-VL-30B			GPT-5.2			Gemini-2.5-Pro		
	OR	RR	OI	OR	RR	OI	OR	RR	OI	OR	RR	OI	OR	RR	OI	OR	RR	OI
Photo	100.00	59.42	98.75	100.00	77.67	99.75	100.00	50.25	99.25	100.00	64.58	99.00	100.00	99.50	99.25	100.00	92.67	98.25
Art Painting	98.00	50.25	96.75	99.50	63.50	97.50	99.50	50.08	98.00	98.50	55.08	98.50	98.50	99.50	97.50	100.00	94.17	97.00
Cartoon	99.50	51.42	97.00	99.00	70.08	98.00	100.00	50.25	97.75	100.00	60.67	97.75	100.00	98.17	97.75	100.00	90.33	98.25
Sketch	94.50	52.25	92.75	96.50	57.25	86.25	96.50	50.42	87.00	96.00	52.83	91.00	94.50	92.25	95.50	97.50	86.50	96.00
Random guess	50.00	50.00	50.00	50.00	50.00	50.00	50.00	50.00	50.00	50.00	50.00	50.00	50.00	50.00	50.00	50.00	50.00	50.00

Table 3: **Performance across task formulations on PACS.** Accuracy is reported for object recognition (OR), object identification (OI), and rotation recognition (RR) tasks (Sec. 3.2.5) across PACS domains. For each model and domain, the best and worst task performances are highlighted in teal and red, respectively. While models perform near-perfectly on OR and OI, performance drops significantly on RR, highlighting a gap between semantic recognition and geometric reasoning.

Dataset	Qwen2.5-VL-7B			Qwen2.5-VL-32B			Qwen3-VL-8B			Qwen3-VL-30B			GPT-5.2			Gemini-2.5-Pro		
	Acc.	TNR	TPR	Acc.	TNR	TPR	Acc.	TNR	TPR	Acc.	TNR	TPR	Acc.	TNR	TPR	Acc.	TNR	TPR
Times New Roman	100.00	100.00	100.00	100.00	100.00	100.00	100.00	100.00	100.00	100.00	100.00	100.00	100.00	100.00	100.00	100.00	100.00	100.00
Handwritten English	99.04	98.08	100.00	99.04	98.08	100.00	100.00	100.00	100.00	99.04	98.08	100.00	99.04	98.08	100.00	99.04	98.08	100.00
Omniglot	81.33	99.88	62.78	96.95	94.52	99.38	99.72	99.45	100.00	99.57	99.88	99.26	98.77	97.54	100.00	96.67	93.35	100.00
Random guess	50.00	50.00	50.00	50.00	50.00	50.00	50.00	50.00	50.00	50.00	50.00	50.00	50.00	50.00	50.00	50.00	50.00	50.00

Table 4: **Model performance for the identity transformation on printed and handwritten scripts.** All models achieve perfect performance on the Times New Roman dataset. The models achieve near-perfect performance on the Handwritten English dataset with a few mistakes in the negative case. The worst performances across all models occur with the Omniglot dataset.

**Findings:** From Table 3, we note that all models achieve near-perfect performance on object recognition (OR) and object identification (OI) across domains, whereas rotation recognition (RR) performance is substantially lower. For instance, in the Photo domain, RR accuracy is 59.42% and 77.67% for Qwen2.5-VL-7B and Qwen2.5-VL-32B, but drops to 50.25% for Qwen3-VL-8B, compared to near-perfect performance on OR and OI. This trend persists across all domains, with RR consistently lower than OR and OI, with the exception of GPT-5.2. The finding is clear: models achieve near-perfect accuracy on object recognition (OR) and identification (OI) tasks while performance collapses on rotation recognition (RR) where such explicit cues are absent. This divergence suggests that models rely on semantic recognition as a shortcut rather than genuine transformation reasoning.

### Takeaways from Studying Rotational Invariance of VLMs

1. VLMs fail ungracefully when presented with images which are rotated variants of each other across datasets, model capacities, and prompts.
2. All models, across different capacities, perform well on real-world photos and the worst on symbolic sketches, indicating lack of true geometric understanding.
3. The underlying visual encoder of Qwen2.5-VL-7B appears to retain the invariance, but this signal is lost when paired with language decoder.
4. Models rely on semantic recognition as a shortcut rather than true transformation reasoning.

### 3.3 Is this behavior specific to rotation transformation?

#### 3.3.1 Case Study 1: Identity Transformation

We begin with a basic visual task: given **two identical images** of the same character or object, can present day VLMs identify that they are the same? We study this question using the Omniglot, Times New Roman, and Handwritten English datasets listed in Sec. 3.1.1, using the following prompt :

**Identity Prompt:** *Are these the same characters? Answer in curly brackets, e.g. {Yes} or {No}.*

**Results.** Table 4 reports model performance on the identity task. Times New Roman achieves 100% accuracy across all six models, and Handwritten English follows closely with 99.04%. For Omniglot, all models achieve near-perfect performance with the exception of Qwen2.5-VL-7B, which records a TPR of 62.78%, indicating that it incorrectly rejects a substantial fraction of identical character pairs. We show 4 random visual examples in Fig. 3 where Qwen2.5-VL-7B fails to identify that the two images are identical. We believe that the performance collapse of Qwen2.5-VL-7B on Omniglot on a simple identity matching task indicates its lack of geometric grounding. It confirms that the model’s success is anchored in script-specific memorization rather than true geometric reasoning.

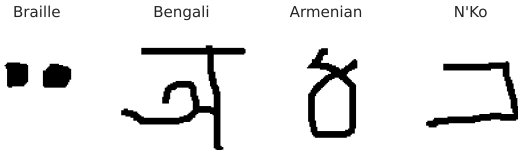


Figure 3: Failure cases on the identity task (Sec. 3.3.1) for Qwen2.5-VL-7B. We show four randomly selected examples from Omniglot dataset where the model incorrectly predicts that two identical inputs correspond to different characters.

Dataset	Qwen2.5-VL-7B			Qwen2.5-VL-32B			Qwen3-VL-8B			Qwen3-VL-30B			GPT-5.2			Gemini-2.5-Pro		
	Acc.	TNR	TPR	Acc.	TNR	TPR	Acc.	TNR	TPR	Acc.	TNR	TPR	Acc.	TNR	TPR	Acc.	TNR	TPR
Times New Roman	98.80	97.60	100.00	99.76	99.52	100.00	100.00	100.00	100.00	98.79	97.59	100.00	98.79	99.03	98.55	99.51	100.00	99.03
Handwritten English	96.77	95.56	97.98	95.36	92.34	98.39	97.59	95.19	100.00	97.59	99.03	96.15	98.07	98.07	98.07	96.63	98.07	95.19
Omniglot	77.40	92.99	61.81	74.21	67.87	80.55	76.05	97.11	54.99	77.04	95.44	58.64	79.72	93.20	66.23	82.56	90.11	75.01
Random guess	50.00	50.00	50.00	50.00	50.00	50.00	50.00	50.00	50.00	50.00	50.00	50.00	50.00	50.00	50.00	50.00	50.00	50.00

Table 5: Model performance on the scale-invariance task aggregated across all scales. All models achieve near-perfect performance on Times New Roman and Handwritten English characters, indicating robustness to scale changes. In contrast, performance on Omniglot is substantially lower and exhibits greater variation in recall (TPR) and specificity (TNR) across models.

### 3.3.2 Case Study 2: Scale Invariance

An ideal MLLM should recognize a character’s identity invariant of scale, performing consistently across both familiar (Latin) and unfamiliar (Mongolian) scripts. We study this on Times New Roman, Handwritten English, and Omniglot (Lake et al., 2015) (Sec. 3.1.1). Each sample pairs a full-resolution reference image (1.0×) with a query image containing a character—either identical or different—at a reduced scale  $s \in \{0.1, 0.3, 0.5, 0.9\}$ . Scaled characters are padded with white pixels to maintain original image dimensions (Fig. 1) (more details in suppl.). We use the following prompt:

**Scale prompt.** Compare the two images and decide if they show the same character. Ignore differences in scale, size, or resolution. Answer with exactly YES or NO.

**Findings:** From Table 5, we observe that Times New Roman achieves near-perfect performance (> 98%) across all models, with both recall and specificity remaining high, indicating that models reliably identify characters across scales. Handwritten English follows closely, with all models exceeding 95% accuracy. Performance drops substantially for Omniglot scripts, with accuracy ranging from 74.21% (Qwen2.5-VL-32B) to 82.56% (Gemini-2.5-Pro). Within Omniglot, for Qwen2.5-VL-7B, more familiar scripts such as Greek (TPR = 70.83%) achieve substantially higher recall than less familiar scripts such as Braille (TPR = 3.85%), while specificity remains near 100% (more in Suppl.). Overall, these results indicates that the performance is strongly driven by script familiarity, with models reliably recognizing scaled variants of familiar scripts but performing poorly on less familiar ones.

### 3.4 Understanding VLMs fragility to simple transformations

**Thinking trace comparison for Gemini-2.5-Pro**

**Rotation prompt:** If I rotate the first image, can I get the second image? Answer in curly brackets, e.g. {Yes} or {No}.

**Times New Roman**

*Thinking trace:*  
Assessing the Images  
I’ve determined both images represent forms of “C” and are now noting stylistic differences.

*Confirming Image Similarity*  
The images are confirmed as rotations of a ‘C’, with careful serif and thickness matching, confirming the 90 degree rotation.

**Response:** {Yes}

**Omniglot**

*Thinking trace:*  
Assessing the Images  
I’ve initiated the analysis, aiming to ascertain the rotation required for image comparison and deliver a definitive answer.

*Comparing Character Forms*  
I’ve examined the images’ structure, tracing each character, and tested rotations without finding a match, deeming them likely different.

**Response:** {No}

To this end, we examine Gemini-2.5-Pro’s (Comanici et al., 2025) reasoning traces on 90° rotation tasks (Sec. 3.2) by comparing familiar Times New Roman characters with unfamiliar Gujarati (Omniglot) characters. For the familiar character “C,” notice that the model identifies the letter’s identity *before* confirming the rotation. Conversely, for the unfamiliar Gujarati character, the model adopts a more low-level structural analysis of the character’s

Script	ICL Setting	Qwen2.5-VL-7B		Qwen2.5-VL-32B		Qwen3-VL-8B		Qwen3-VL-30B		GPT-5.2		Gemini-2.5-Pro	
		TNR	TPR	TNR	TPR	TNR	TPR	TNR	TPR	TNR	TPR	TNR	TPR
Malayalam (top-tier)	None	100.00	00.00	97.87	06.38	100.00	00.00	100.00	02.13	93.62	34.04	100.00	38.30
	Few-shot	100.00	00.00	65.96	51.06↑	100.00	34.04↑	78.72	72.34↑	91.49	85.11↑	97.87	34.04↓
	Rotational Grid	100.00	00.00	91.49	12.77↑	65.96	65.96↑	23.40	87.23↑	72.34	97.87↑	93.62	48.94↑
Tengwar (medium-tier)	None	100.00	00.00	88.00	16.00	100.00	00.00	100.00	00.00	100.00	20.00	96.00	32.00
	Few-shot	100.00	00.00	68.00	76.00↑	100.00	16.00↑	68.00	72.00↑	80.00	68.00↑	92.00	32.00
	Rotational Grid	100.00	00.00	88.00	24.00↑	72.00	88.00↑	40.00	76.00↑	60.00	88.00↑	88.00	56.00↑
Braille (bottom-tier)	None	100.00	00.00	65.38	15.38	100.00	00.00	100.00	03.85	100.00	07.69	100.00	50.00
	Few-shot	100.00	00.00	88.46	19.23↑	100.00	11.54↑	92.31	50.00↑	92.31	73.08↑	96.15	26.92↓
	Rotational Grid	100.00	00.00	100.00	00.00↓	100.00	11.54↑	73.08	50.00↑	69.23	65.38↑	100.00	46.15↓

Table 6: **Model performance with in-context learning and structured visual prompting across scripts.** Arrows indicate change in TPR relative to the *None* setting: ↑ denotes improvement and ↓ denotes degradation. Both few-shot prompting and rotational grid inputs increase TPR across models, but often reduce TNRs. Improvements are larger for higher-capacity models.

geometry. We make a similar observation upon analyzing thinking traces of several other unfamiliar scripts. While this shift to structural analysis on unfamiliar scripts mirrors how humans *might* solve a similar problem, Gemini-2.5-Pro’s subsequent performance drop reveals a critical deficiency: current VLMs *lack the robust geometric reasoning required to succeed without semantic anchors*.

### 3.5 Can transformation invariance be instilled?

**In-Context Learning (ICL).** Having established that MLLMs fail systematically on transformation tasks, we now investigate if in-context learning (ICL) (Brown et al., 2020) and structured visual prompting can mitigate these errors. We evaluate across three representative Omniglot scripts, selected based on their performance on the rotation invariance task (Sec. 3.2.2): Malayalam (top-tier), Tengwar (medium-tier), and Braille (bottom-tier). To the system prompt, we prepend two labeled examples: a positive pair with the caption “*This is Image B, which is a rotated version of Image A,*” and a negative pair labeled “*This is Image D, which is NOT a rotated version of Image C.*” The positive example uses Angelic script characters (Images A and B); the negative uses an Angelic character as *Image C* and a Gujarati character as the rotated variant (*Image D*) (see suppl. material).

**Findings:** From Table 6, ICL improves performance primarily through increases in TPR, even with only **two** example pairs. For instance, Qwen2.5-VL-32B improves from 6.38% to 51.06% on Malayalam, while GPT-5.2 improves from 34.04% to 85.11%. However, these gains often come at the cost of reduced TNR (e.g., Qwen2.5-VL-32B drops from 97.87% to 65.96% for Malayalam), indicating increased false positives. Improvements remain limited for smaller models such as Qwen2.5-VL-7B, where TPR remains zero.

**Rotational Grid.** As done in RotBench (Niu et al., 2026), we construct a single composite image showing a character at four rotation angles: 0°, 90°, 180°, 270°. We use characters from Angelic and Gujarati, both mid-performing scripts, to construct the grid. We then prepend this image and a prompt describing the grid (see suppl. material) with the rotation task prompt in Sec. 3.2.2.

**Findings:** From Table 6, rotational grid increases TPR but causes larger drops in TNR than ICL. For example, the TPR of Qwen3-VL-8B improves from 0.00% to 65.96% on Malayalam, but TNR drops from 100.00% to 65.96%. Similarly, Qwen3-VL-30B improves from 2.13% to 87.23%, at the cost of TNR plummeting to 23.40%. Even GPT-5.2 follows this pattern, achieving a near-perfect 97.87% TPR but with a degraded TNR of 72.34%.

From these two experiments, it is clear that both approaches help instill *some* but not a robust understanding of rotation recognition. While we hypothesized that ICL and the rotational grid would provide the visual evidence necessary to map the input across different angles, it appears to make the high-capacity models “over-eager” and induce a confirmation bias that spikes TPR at the expense of discriminative accuracy.

## 4 Conclusion

This work disentangles the geometric reasoning and semantic familiarity of state-of-the-art vision-language models. Across three transformations, four visual domains, and six models, we demonstrate that while performance is robust on semantically rich, familiar inputs (e.g., natural images), it degrades sharply on sketches, symbolic characters, and unfamiliar

scripts. These failures persist regardless of model architecture, scale, or prompting strategy, and are only partially mitigated by in-context learning or structured visual prompts. Our findings reveal that current VLMs lack a fundamental, invariant grasp of geometry and instead rely on “semantic anchors” to navigate spatial tasks. Future research must move beyond surface-level data familiarity, exploring architectural innovations and targeted data augmentations that instill true, zero-shot geometric reasoning capabilities.

**Acknowledgments.** We thank Thomas Fel for especially helpful discussions. We also thank Dana Arad, David Bau, and Arsha Nagrani for helpful discussions and feedback, and, Dahye Kim, Chaitanya Chakka, and Manushree Vasu from our research group at BU for helpful discussions and feedback.

## References

- Shuai Bai, Yuxuan Cai, Ruizhe Chen, Keqin Chen, Xionghui Chen, Zesen Cheng, Lianghao Deng, Wei Ding, Chang Gao, Chunjiang Ge, et al. Qwen3-v1 technical report, 2025a. URL <https://arxiv.org/abs/2511.21631>.
- Shuai Bai, Keqin Chen, Xuejing Liu, Jialin Wang, Wenbin Ge, Sibao Song, Kai Dang, Peng Wang, Shijie Wang, Jun Tang, et al. Qwen2.5 technical report, 2025b. URL <https://arxiv.org/abs/2412.15115>.
- Tom Brown, Benjamin Mann, Nick Ryder, Melanie Subbiah, Jared D Kaplan, Prafulla Dhariwal, Arvind Neelakantan, Pranav Shyam, Girish Sastry, Amanda Askell, et al. Language models are few-shot learners. *Advances in neural information processing systems*, 33:1877–1901, 2020.
- Declan Campbell, Sunayana Rane, Tyler Giallanza, Nicolò De Sabbata, Kia Ghods, Amogh Joshi, Alexander Ku, Steven M. Frankland, Thomas L. Griffiths, Jonathan D. Cohen, and Taylor W. Webb. Understanding the limits of vision language models through the lens of the binding problem, 2025. URL <https://arxiv.org/abs/2411.00238>.
- Shivam Chandhok, Wan-Cyuan Fan, Vered Shwartz, Vineeth N Balasubramanian, and Leonid Sigal. Response wide shut? surprising observations in basic vision language model capabilities. In *Proceedings of the 63rd Annual Meeting of the Association for Computational Linguistics (Volume 1: Long Papers)*, pp. 25530–25545, 2025.
- Liang Chen, Weichu Xie, Yiyang Liang, Hongfeng He, Hans Zhao, Zhibo Yang, Zhiqi Huang, Haoning Wu, Haoyu Lu, Y. Charles, Yiping Bao, Yuantao Fan, Guopeng Li, Haiyang Shen, Xuanzhong Chen, Wendong Xu, Shuzheng Si, Zefan Cai, Wenhao Chai, Ziqi Huang, Fangfu Liu, Tianyu Liu, Baobao Chang, Xiaobo Hu, Kaiyuan Chen, Yixin Ren, Yang Liu, Yuan Gong, and Kuan Li. Babyvision: Visual reasoning beyond language, 2026. URL <https://arxiv.org/abs/2601.06521>.
- Gheorghe Comanici, Eric Bieber, Mike Schaeckermann, Ice Pasupat, Noveen Sachdeva, Inderjit Dhillon, Marcel Blistein, Ori Ram, Dan Zhang, Evan Rosen, et al. Gemini 2.5: Pushing the frontier with advanced reasoning, multimodality, long context, and next generation agentic capabilities. *arXiv preprint arXiv:2507.06261*, 2025.
- Peijian Ding, Davit Soselia, Thomas Armstrong, Jiahao Su, and Furong Huang. Reviving shift equivariance in vision transformers, 2023. URL <https://arxiv.org/abs/2306.07470>.
- Haiwen Feng, Long Lian, Lisa Dunlap, Jiahao Shu, XuDong Wang, Renhao Wang, Trevor Darrell, Alane Suhr, and Angjoo Kanazawa. Visually prompted benchmarks are surprisingly fragile. *arXiv preprint arXiv:2512.17875*, 2025.
- Hongcheng Gao, Zihao Huang, Lin Xu, Jingyi Tang, Xinhao Li, Yue Liu, Haoyang Li, Taihang Hu, Minhua Lin, Xinlong Yang, Ge Wu, Balong Bi, Hongyu Chen, and Wentao Zhang. Pixels, patterns, but no poetry: To see the world like humans, 2025. URL <https://arxiv.org/abs/2507.16863>.
- Arshia Hemmat, Adam Davies, Tom Lamb, Jianhao Yuan, Philip Torr, Ashkan Khakzar, and Francesco Pinto. Hidden in plain sight: evaluating abstract shape recognition in vision-language models. *Advances in Neural Information Processing Systems*, 37:88527–88556, 2024.
- Dahye Kim, Xavier Thomas, and Deepti Ghadiyaram. Revelio: Interpreting and leveraging semantic information in diffusion models. In *Proceedings of the IEEE/CVF International Conference on Computer Vision*, pp. 4659–4669, 2025.
- Risi Kondor and Shubhendu Trivedi. On the generalization of equivariance and convolution in neural networks to the action of compact groups, 2018. URL <https://arxiv.org/abs/1802.03690>.

- Brenden M. Lake, Ruslan Salakhutdinov, and Joshua B. Tenenbaum. Human-level concept learning through probabilistic program induction. *Science*, 350(6266):1332–1338, 2015. doi: 10.1126/science.aab3050. URL <https://www.science.org/doi/abs/10.1126/science.aab3050>.
- Hugo Laurençon, Léo Tronchon, Matthieu Cord, and Victor Sanh. What matters when building vision-language models? *Advances in Neural Information Processing Systems*, 37:87874–87907, 2024.
- Xiaoqi Li, Mingxu Zhang, Yiran Geng, Haoran Geng, Yuxing Long, Yan Shen, Renrui Zhang, Jiaming Liu, and Hao Dong. Manipllm: Embodied multimodal large language model for object-centric robotic manipulation. In *Proceedings of the IEEE/CVF Conference on Computer Vision and Pattern Recognition*, pp. 18061–18070, 2024.
- Haotian Liu, Chunyuan Li, Qingyang Wu, and Yong Jae Lee. Visual instruction tuning. In *NeurIPS*, 2023.
- Sujay Mann. Handwritten english characters and digits, 2024. URL <https://www.kaggle.com/datasets/sujaymann/handwritten-english-characters-and-digits>. Accessed: 2026-03-29.
- Sebastian Ray Mason, Anders Gjørbye, Phillip Chavarria Højbjerg, Lenka Tětková, and Lars Kai Hansen. Large vision models can solve mental rotation problems, 2026. URL <https://arxiv.org/abs/2509.15271>.
- Stanley Morison and Victor Lardent. Times new roman. [https://en.wikipedia.org/wiki/Times\\_New\\_Roman](https://en.wikipedia.org/wiki/Times_New_Roman), 1932. Typeface originally commissioned for *The Times* newspaper. Accessed: 2026-03-30.
- Tianyi Niu, Jaemin Cho, Elias Stengel-Eskin, and Mohit Bansal. Rotbench: Evaluating multimodal large language models on identifying image rotation, 2026. URL <https://arxiv.org/abs/2508.13968>.
- OpenAI. Gpt-5 system card. Technical report, OpenAI, December 2025. URL [https://cdn.openai.com/pdf/3a4153c8-c748-4b71-8e31-aecbde944f8d/oai\\_5\\_2\\_system-card.pdf](https://cdn.openai.com/pdf/3a4153c8-c748-4b71-8e31-aecbde944f8d/oai_5_2_system-card.pdf). Accessed: 2025-3-4.
- Maxime Oquab, Timothée Darcet, Théo Moutakanni, Huy Vo, Marc Szafraniec, Vasil Khalidov, Pierre Fernandez, Daniel Haziza, Francisco Massa, Alaaeldin El-Nouby, Mahmoud Assran, Nicolas Ballas, Wojciech Galuba, Russell Howes, Po-Yao Huang, Shang-Wen Li, Ishan Misra, Michael Rabbat, Vasu Sharma, Gabriel Synnaeve, Hu Xu, Hervé Jegou, Julien Mairal, Patrick Labatut, Armand Joulin, and Piotr Bojanowski. Dinov2: Learning robust visual features without supervision, 2024. URL <https://arxiv.org/abs/2304.07193>.
- Alec Radford, Jong Wook Kim, Chris Hallacy, Aditya Ramesh, Gabriel Goh, Sandhini Agarwal, Girish Sastry, Amanda Askell, Pamela Mishkin, Jack Clark, Gretchen Krueger, and Ilya Sutskever. Learning transferable visual models from natural language supervision, 2021. URL <https://arxiv.org/abs/2103.00020>.
- Santhosh Kumar Ramakrishnan, Erik Wijmans, Philipp Kraehenbuehl, and Vladlen Koltun. Does spatial cognition emerge in frontier models?, 2025. URL <https://arxiv.org/abs/2410.06468>.
- R. Rombach, A. Blattmann, D. Lorenz, P. Esser, and B. Ommer. High-resolution image synthesis with latent diffusion models. In *CVPR*, 2022.
- An Vo, Khai-Nguyen Nguyen, Mohammad Reza Taesiri, Vy Tuong Dang, Anh Totti Nguyen, and Daeyoung Kim. Vision language models are biased, 2025. URL <https://arxiv.org/abs/2505.23941>.
- Andrew B Watson. Perimetric complexity of binary digital images: Notes on calculation and relation to visual complexity. Technical report, 2011.

Antonia Wüst, Tim Woydt, Lukas Helff, Inga Ibs, Wolfgang Stammer, Devendra S Dhami, Constantin A Rothkopf, and Kristian Kersting. Bongard in wonderland: Visual puzzles that still make ai go mad? arXiv preprint arXiv:2410.19546, 2024.

E Yiu, M Qraitem, C Wong, AN Majhi, Y Bai, S Ginosar, A Gopnik, and K Saenko. Kiva: Kid-inspired visual analogies for testing large multimodal models (version 1). arxiv, 2024.

Samuel Yu, Peter Wu, Paul Pu Liang, Ruslan Salakhutdinov, and Louis-Philippe Morency. Pacs: A dataset for physical audiovisual commonsense reasoning, 2022. URL <https://arxiv.org/abs/2203.11130>.

Xiaohua Zhai, Basil Mustafa, Alexander Kolesnikov, and Lucas Beyer. Sigmoid loss for language image pre-training. In Proceedings of the IEEE/CVF international conference on computer vision, pp. 11975–11986, 2023.

Junyi Zhang, Charles Herrmann, Junhwa Hur, Eric Chen, Varun Jampani, Deqing Sun, and Ming-Hsuan Yang. Telling left from right: Identifying geometry-aware semantic correspondence. In Proceedings of the IEEE/CVF Conference on Computer Vision and Pattern Recognition (CVPR), pp. 3076–3085, June 2024.

## Supplementary Material for “Semantic Richness or Geometric Reasoning? The Fragility of VLM’s Visual Invariance”

### Table of Contents

<b>A.</b>	Dataset Examples .....	15
	<b>A.1</b> Dataset overview .....	15
	<b>A.2</b> Omniglot Dataset .....	16
	<b>A.3</b> PACS Dataset .....	17
	<b>A.4</b> Times New Roman Dataset .....	18
	<b>A.5</b> Handwritten English Dataset .....	19
<b>B.</b>	Preprocessing and Transformations .....	20
<b>C.</b>	Vision encoders studied for rotational invariance .....	21
<b>D.</b>	Interaction with the Language Decoder .....	22
<b>E.</b>	PACS Performance for the Scale Invariance Task .....	23
<b>F.</b>	Perimetric Complexity Analysis .....	24
<b>G.</b>	Additional Scale Invariance Analysis .....	25
<b>H.</b>	ICL and Rotational Grid Setup .....	26
	<b>H.1</b> Few-Shot Setup .....	26
	<b>H.2</b> Rotational Grid Setup .....	27
<b>I.</b>	Additional Results .....	28
	<b>I.1</b> Rotation recognition performance across character datasets .....	28
	<b>I.2</b> PACS rotation results for $10^\circ$ – $90^\circ$ .....	28
	<b>I.3</b> PACS identity experiment results .....	28
	<b>I.4</b> Model performance with In-Context Learning .....	29

## A Dataset Examples

### A.1 Dataset overview

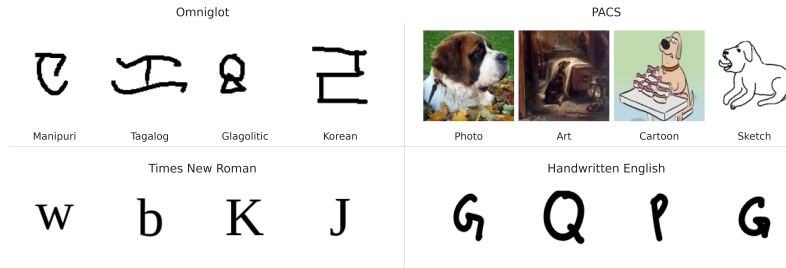


Figure 4: **Datasets used in our evaluation.** Omniglot (Lake et al., 2015) contains handwritten binary characters from 50 diverse scripts. Times New Roman (Morison & Lardent, 1932) provides standardized English characters rendered in a fixed typeface. Handwritten English Mann (2024) includes handwritten characters from the English alphabet. PACS (Yu et al., 2022) contains images of common object categories (e.g., guitar, dog, elephant) across four visual domains: Photograph, Art, Cartoon, and Sketch. Together, these datasets allow us to evaluate transformation invariance in MLLMs across scripts, visual styles, and images with varying levels of semantic richness.

Dataset	# Samples	Description
Omniglot	1,623	Handwritten characters across 50 scripts
Times New Roman	52	Printed English alphabet (A–Z, a–z)
Handwritten English	52	Handwritten English alphabet
PACS	800	4 domains × 200 images each

Table 7: **Dataset overview.** Number of samples used for evaluation in each dataset.

Omniglot scripts			
Alphabet of the Magi	Armenian	Gujarati	Mongolian
Angelic	Asomtavruli (Georgian)	Gurmukhi	N’Ko
Anglo-Saxon Futhorc	Atemayar Qelisyayer	Hebrew	Ojibwe (Canadian Aboriginal)
Arcadian	Atlantean	Inuktitut (Canadian Aboriginal)	Old Church Slavonic (Cyrillic)
Aurek-Besh	Avesta	Japanese (Hiragana)	Oriya
Balinese	Bengali	Japanese (Katakana)	Sanskrit
Blackfoot (Canadian Aboriginal)	Braille	Kannada	Sylheti
Burmese (Myanmar)	Cyrillic	Keble	Syriac (Estrangelo)
Early Aramaic	Futurama	Korean	Syriac (Serto)
Ge’ez	Glagolitic	Latin	Tagalog
Grantha	Greek	Malay (Jawi - Arabic)	Tengwar
Malayalam	Manipuri	Mkhedruli (Georgian)	Tibetan
Tifinagh	ULOG		

Table 8: **Omniglot scripts.** List of 50 writing systems used in the Omniglot dataset.

<b>Categories</b>	Dog, Elephant, Giraffe, Horse, Person, Guitar, House
<b>Domains</b>	Photograph, Art Painting, Cartoon, Sketch

Table 9: **PACS dataset.** Object categories and visual domains used in evaluation.

## A.2 Omniglot Dataset



Figure 5: Examples from the Omniglot dataset

### A.3 PACS Dataset

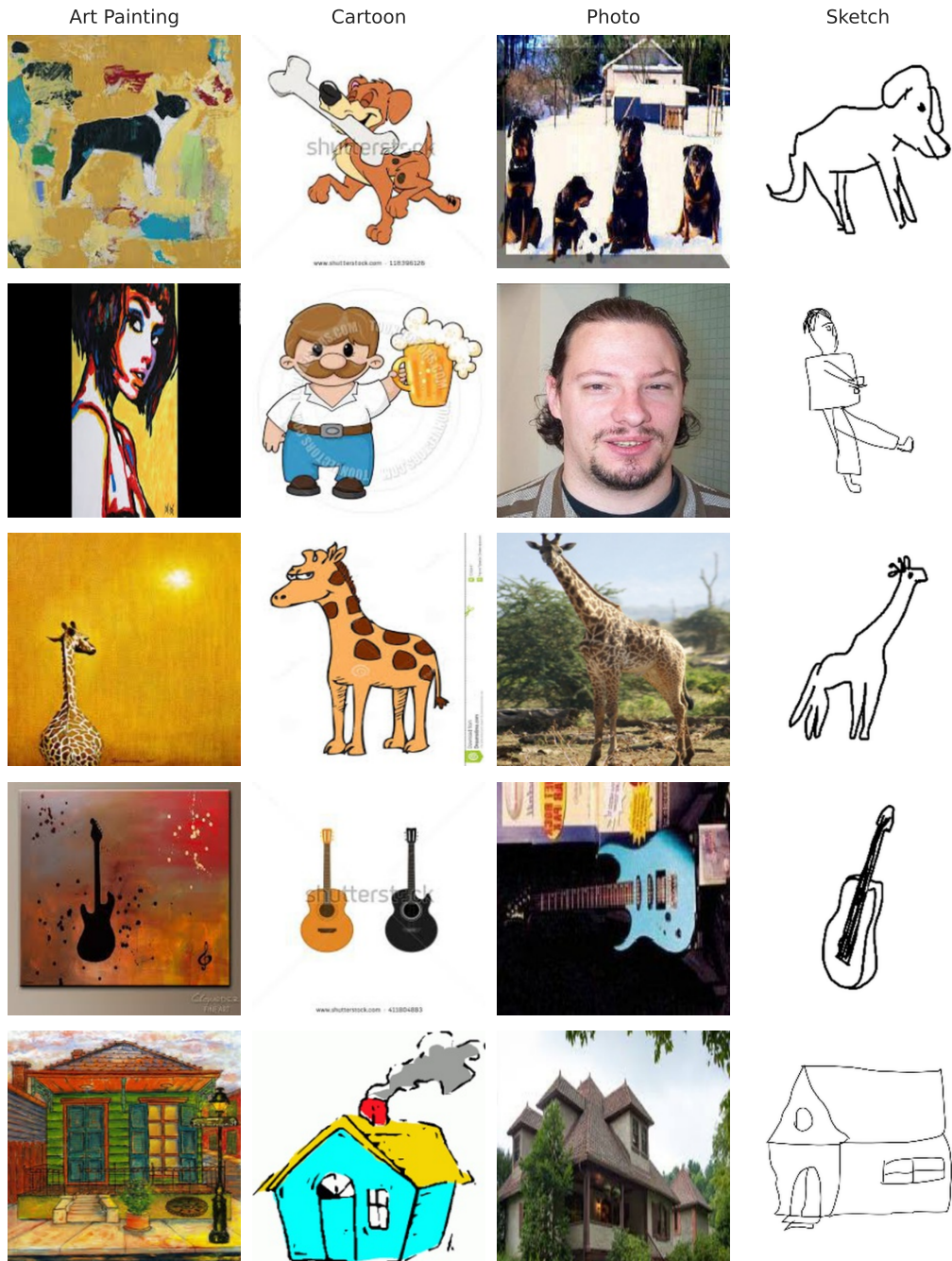


Figure 6: Examples from the PACS dataset

#### A.4 Times New Roman Dataset

Y w a C Q  
g f Z T e  
W l N u I  
S o G v J

Figure 7: Examples from the Times New Roman dataset

## A.5 Handwritten English Dataset

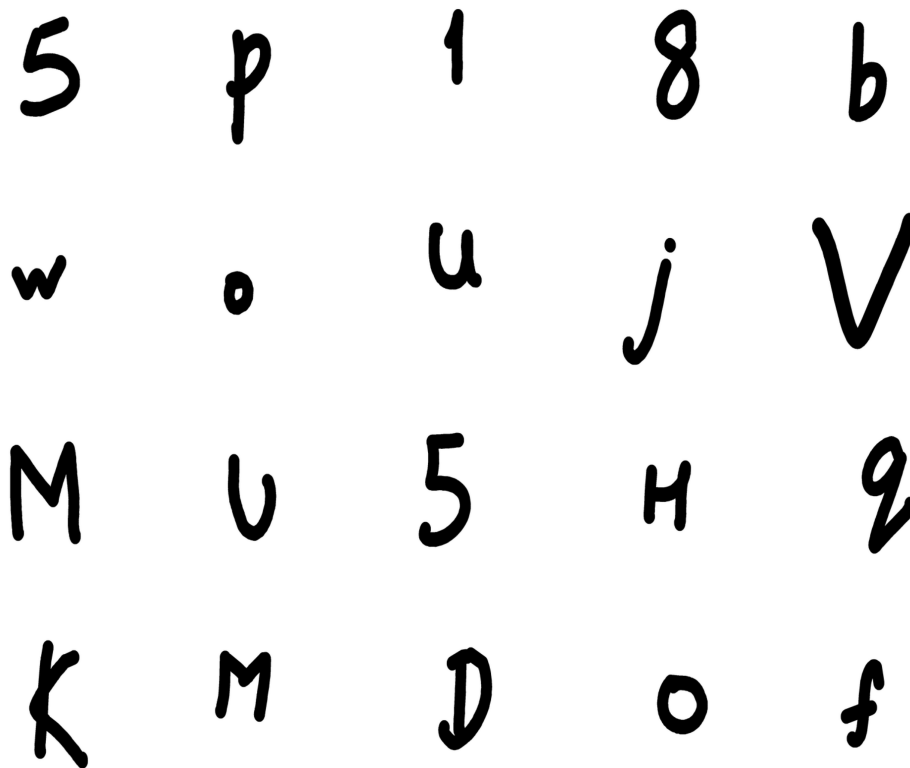


Figure 8: Examples from the Handwritten English dataset

## B Preprocessing and Transformations

For rotation (Sec. 3.2.2) and scale experiments (Sec. 3.3.2), transformations are applied about the image center. Non-orthogonal rotations introduce empty regions where no original pixels are present (Fig. 9); these regions are filled with white padding pixels for the character datasets (Omniglot, Times New Roman, and Handwritten English) and for PACS. For scale transformations, characters are resized by a factor  $s \in \{0.1, 0.3, 0.5, 0.9\}$  and padded to maintain the original image dimensions (Fig. 9). In the character datasets, images are already represented on a white background, so padding introduced by transformations is consistent with the background of the original images. In contrast, for PACS, scale transformations and non-orthogonal rotations introduce visible white padding regions. We acknowledge this as a dataset-dependent artifact that may influence model behavior. However, for the main analysis in Table 2, we restrict rotations to  $90^\circ$ ,  $180^\circ$ , and  $270^\circ$ , which avoids introducing such padding artifacts.

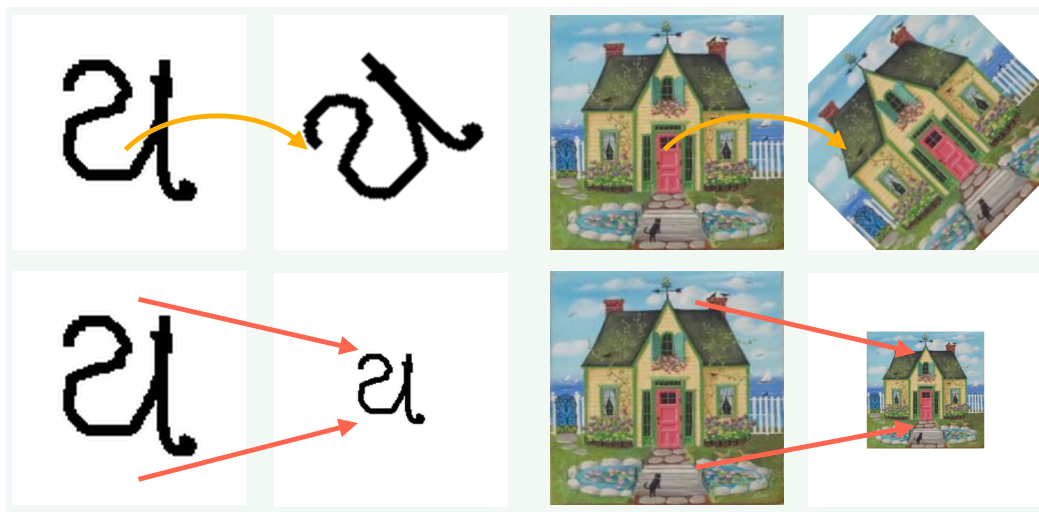


Figure 9: **Padding artifacts under rotation and scaling.** Top row shows rotation and bottom row shows scaling. Non- $90^\circ$  rotations introduce padding regions corresponding to pixels not covered by the original image. Scaling similarly introduces padding for resized images. For character datasets (left), padding matches the white background and is not visually salient. In contrast, for PACS (right), padding introduces visible artifacts under both rotation and scaling. Top row: Images rotated by  $45^\circ$ . Bottom row: Images scaled by 0.5.

### C Vision encoders studied for rotational invariance (Sec. 3.2.1)

Model	Feature Extraction	Dimension
CLIP (ViT-L/14) (Radford et al., 2021)	CLS token	768
DINOv2 (ViT-L/14) (Oquab et al., 2024)	CLS token	1024
SigLIP (ViT-SO400M) (Zhai et al., 2023)	MAP (multi-head attention pooling)	1152
Qwen2.5-VL-7B (Bai et al., 2025b)	Mean over vision tokens	3584
Stable Diffusion v2.1 (Rombach et al., 2022)	Mean over layer 14 features	1280

Table 10: **Vision feature extraction details.** For CLIP and DINOv2, we use the CLS token. For SigLIP, we use the multi-head attention pooling (MAP) output. For Qwen2.5-VL, we average vision token embeddings to obtain a global representation. For Stable Diffusion v2.1 we obtain features from layer 14 in the UNet.

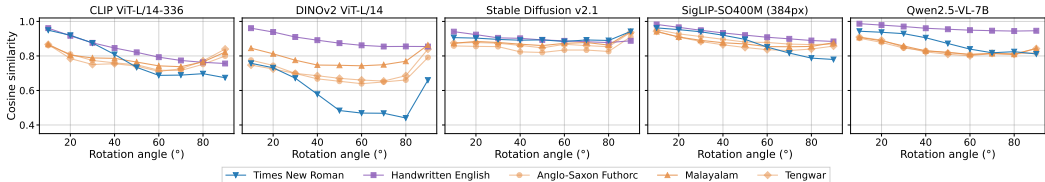


Figure 10: **Cosine similarity between features extracted from different vision encoders** on pairs of images under rotation. Select **Omniglot scripts** are shown in orange, while **Times New Roman** and **Handwritten English** are shown in blue and purple respectively. Across all encoders, similarity decreases with increasing rotation angle, with DINOv2 showing the steepest drop and SigLIP and Qwen2.5-VL-7B maintaining relatively higher similarity.

**CLIP (ViT-L/14) (Radford et al., 2021)** We extract image features using the [CLS] token, which serves as a global representation of the input image. These features are used directly for cosine similarity computations.

**DINOv2 (ViT-L/14) (Oquab et al., 2024)** We extract image features using the [CLS] token, which serves as a global representation of the input image. These features are used directly for cosine similarity computations.

**SigLIP (ViT-SO400M) (Zhai et al., 2023)** We use the multi-head attention pooling (MAP) output, which aggregates information across all visual tokens to form a global representation of the input image.

**Qwen2.5-VL-7B (Bai et al., 2025b)** We compute the mean of the vision token embeddings from the final layer to obtain a global image representation, which is then used for cosine similarity computations.

**Stable Diffusion v2.1 (Rombach et al., 2022)** Following prior work (Kim et al., 2025) showing that intermediate layers of diffusion models capture rich semantic information, we extract features from layer 14 of the U-Net encoder and compute their spatial mean to obtain a representative representation.

## D Suspect 4: Interaction with the Language Decoder

Metric	Times New Roman	Handwritten English	Braille	Balinese	Anglo-Saxon_Futhorc	Tengwar	Malayalam	Grantha
Acc.	57.87	54.54	66.43	50.18	53.76	49.63	50.87	50.42
TPR	77.27	95.28	46.85	99.62	97.17	99.27	96.71	99.78
TNR	38.46	13.81	86.01	0.75	10.34	0.00	5.03	1.05

Table 11: **Idefics2 accuracy performance on the rotation task across scripts.** Times New Roman and Handwritten English are shown in blue and purple respectively, while Omniglot scripts are shown in orange. Accuracy remains near chance for most scripts, despite consistently high TPR and substantially lower TNR, indicating a strong “YES” prediction bias.

The analyses in Sec. 3.2.1 reveal a striking disconnect: vision encoders maintain high cosine similarity between a character and its rotated counterpart, yet MLLMs consistently fail to recognize the same rotation (Table 11).

To isolate the contribution of the language decoder, we evaluate Idefics2 (Laurençon et al., 2024), which uses a frozen SigLIP-SO400M-384 (Zhai et al., 2023) vision encoder, the same encoder evaluated in Sec. 3.2.2. This enables a controlled comparison; if SigLIP preserves rotational similarity at the feature level but Idefics2 fails at the task level, the gap likely arises from how these representations are used within the MLLM (i.e., how the language decoder processes and utilizes those visual representations). Table 11 reports Idefics2’s performance on the rotation task across scripts following the same setup as in Sec. 3.2.2. Despite SigLIP maintaining high cosine similarity between rotated character pairs across all scripts (Fig. 2), Idefics2 achieves only near-chance accuracy across all evaluated scripts (~ 50 – 66%). Performance varies widely across scripts and is driven by a strong “YES” bias: TPR is consistently high while TNR is often near zero, indicating frequent false positives. This mismatch shows that while the vision encoder produces highly similar representations for transformed inputs, this similarity alone is insufficient for reliable downstream reasoning about transformations.

## E PACS Performance for the Scale Invariance Task

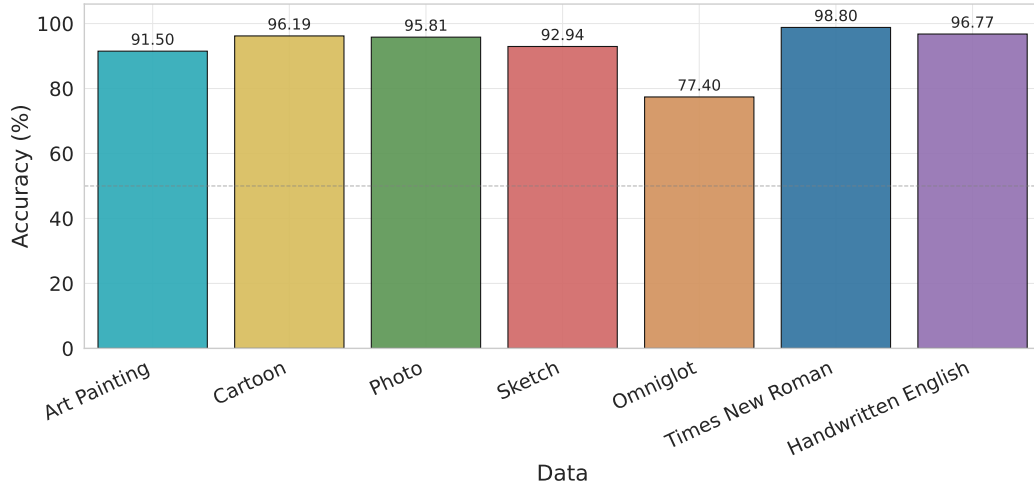


Figure 11: **Scale invariance performance across datasets for Qwen2.5-VL**, aggregated over all scales (Sec. 3.3.2). Performance is high on natural image domains (Art Painting, Cartoon, Photo, Sketch) and familiar scripts (Times New Roman, Handwritten English), but drops on Omniglot, indicating reduced robustness under lower semantic familiarity.

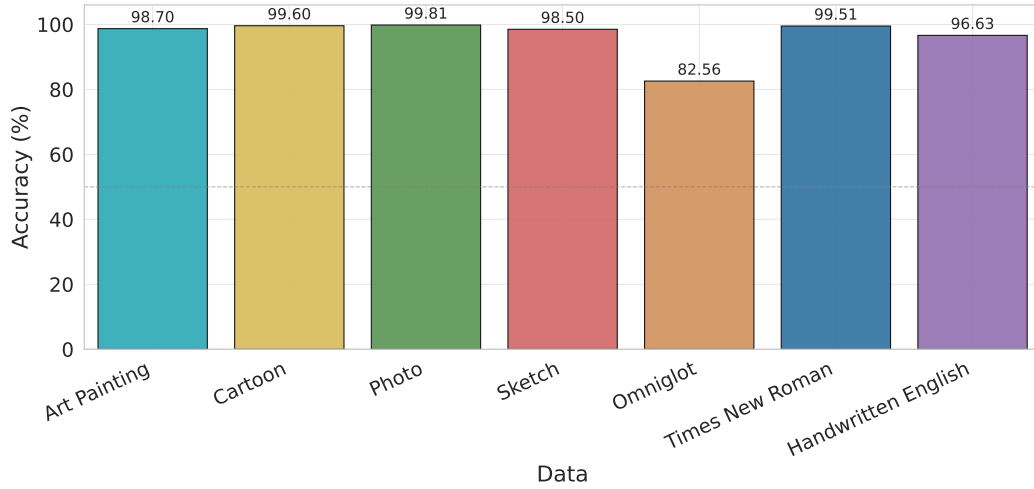


Figure 12: **Scale invariance performance across datasets for Gemini-2.5-Pro**, aggregated over all scales (Sec. 3.3.2). Performance is near-perfect on natural image domains (Art Painting, Cartoon, Photo, Sketch) and familiar scripts (Times New Roman, Handwritten English), but drops on Omniglot, indicating reduced robustness under lower semantic familiarity.

## F Perimetric Complexity Analysis

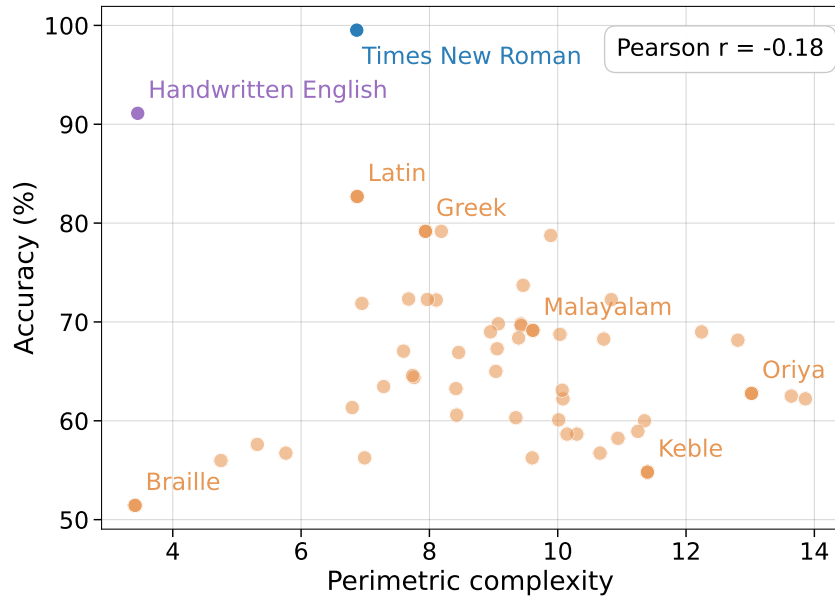


Figure 13: **Perimetric complexity vs performance.** Perimetric complexity shows a weak correlation ( $r = -0.18$ ) with accuracy of Qwen2.5-VL-7B on the scale invariance task. *Times New Roman* and *Handwritten English* are shown in blue and purple respectively, while *Omniglot scripts* are highlighted in orange.

**Visual complexity alone does not account for performance differences across scripts.** We study if the performance struggle is more severe on more visually intricate and complex scripts. To test this hypothesis, we use perimetric complexity as used by Watson (2011), defined as  $P^2/A$ , where  $P$  is the total perimeter of the character and  $A$  is the area occupied by the character. This scale- and orientation-invariant metric indicates structural intricacy. If structural complexity is the primary cause, scripts of higher perimetric complexity would perform worse. However, the Pearson correlation between script-level complexity and mean accuracy is weak ( $r = -0.18$ ), indicating that structural intricacy alone cannot explain the poor performance on unknown scripts.

## G Additional Scale Invariance Analysis

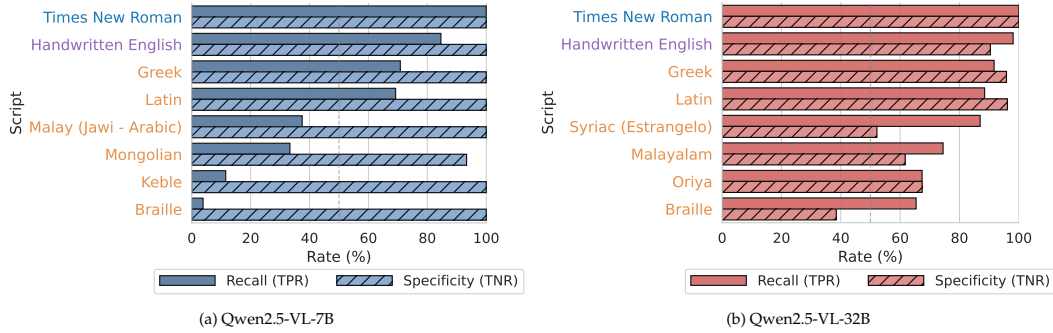


Figure 14: **Recall and Specificity at scale  $0.3\times$  for representative scripts for the scale-invariance task.** English characters rendered in Times New Roman, Handwritten English characters, and Omniglot scripts are shown in blue, purple, and orange respectively, and are selected to represent high-, medium-, and low-performing groups. Across both models, familiar scripts such as Greek and Latin consistently outperform less familiar scripts like Braille. While Qwen2.5-VL-32B achieves higher recall than Qwen2.5-VL-7B on low-performing Omniglot scripts, it exhibits lower specificity.

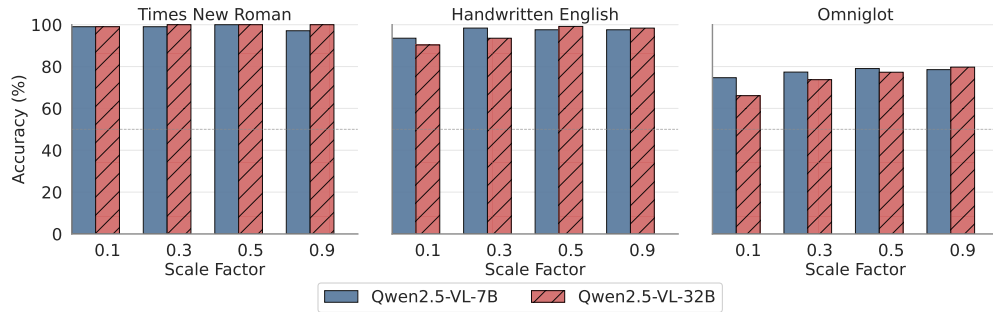


Figure 15: **Model accuracy on the scale-invariance task across scale factors.** Both Qwen2.5-VL-7B and Qwen2.5-VL-32B models maintain near-perfect accuracy for both Times New Roman and Handwritten English characters across all scales, while performance on Omniglot scripts is substantially and consistently lower for both models.

## H ICL and Rotational Grid Setup

### H.1 Few-Shot Setup

**System Prompt:**

You are a vision reasoning model. You will be shown pairs of images. Determine whether one image is a rotated version of the other.

**Examples:**

“This is Image B, which is a rotated version of Image A.”

“This is Image D, which is NOT a rotated version of Image C.”

**Positive Example**

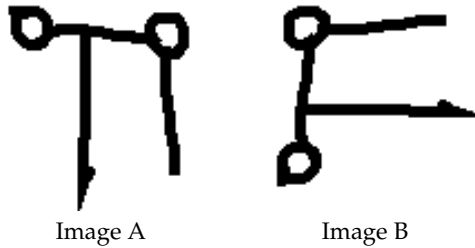


Image A

Image B

**Negative Example**

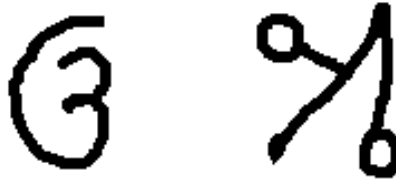


Image C

Image D

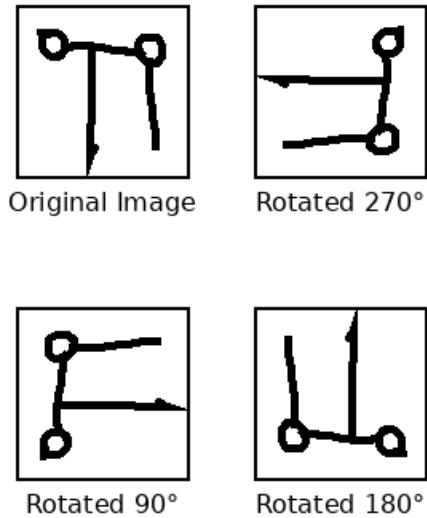
Figure 16: **In-context learning (ICL) prompting setup.** The system prompt includes two labeled examples: a positive pair (top) where one image is a rotated version of the other, and a negative pair (bottom) where the images are not related by rotation.

## H.2 Rotational Grid Setup

**System Prompt:**

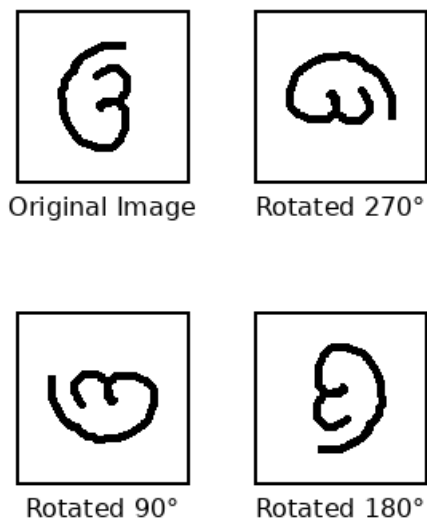
You are a vision reasoning model. You will be shown “Rotational Grids” which display a character in four orientations simultaneously. The layout is: Top-Left: Original Image ( $0^\circ$ ), Top-Right: Rotated  $270^\circ$ , Bottom-Left: Rotated  $90^\circ$ , Bottom-Right: Rotated  $180^\circ$ . Use the labels in the grid to understand the transformation.

**Reference 1: Rotational Grid for Character A**



This grid defines the rotation patterns.

**Reference 2: Rotational Grid for Character B**



This grid defines the rotation patterns.

Figure 17: **Rotational grid prompting setup.** The model is first given a structured system prompt describing the layout of rotational grids. Two reference grids (Character A and Character B) are then provided to illustrate rotations across different characters.

## I Additional Results

### I.1 Rotation recognition performance across character datasets (additional)

Dataset	Qwen2.5-VL-7B			Qwen2.5-VL-32B			Qwen2.5-VL-72B			Qwen3-VL-4B		
	Acc.	TNR	TPR	Acc.	TNR	TPR	Acc.	TNR	TPR	Acc.	TNR	TPR
Times New Roman	50.96	100.00	01.92	54.13	100.00	08.27	52.40	100.00	04.81	50.29	100.00	00.58
Handwritten English	50.96	98.08	03.85	62.50	98.08	26.92	57.21	100.00	14.42	50.00	100.00	00.00
Omniglot	50.70	99.45	01.95	54.20	94.73	13.68	57.48	96.51	18.46	50.24	99.98	00.51
Dataset	Qwen3-VL-8B			Qwen3-VL-30B			GPT-5.2			Gemini-2.5-Pro		
	Acc.	TNR	TPR	Acc.	TNR	TPR	Acc.	TNR	TPR	Acc.	TNR	TPR
Times New Roman	50.19	100.00	00.38	67.12	100.00	34.23	72.31	95.00	49.62	89.23	100.00	78.46
Handwritten English	50.00	100.00	00.00	56.44	100.00	12.88	67.02	96.35	37.69	67.40	99.42	35.38
Omniglot	50.99	99.96	02.03	56.55	99.76	13.34	75.08	80.95	69.21	76.49	98.69	54.29

Table 12: **Rotation recognition performance across character datasets.** Best and worst accuracy per model across datasets are highlighted in teal and red, respectively. Performance aggregated over rotation angles 10°–90°. While TNR remains near-perfect across all models, TPR is consistently low, indicating a failure to recognize rotated variants. Closed-source models perform better than open-source models, but the failure persists across all models. We additionally include results for Qwen2.5-VL-72B and Qwen3-VL-4B.

### I.2 PACS rotation results for 10° - 90°

Domain	Qwen2.5-VL-7B			Qwen2.5-VL-32B			Qwen3-VL-8B			Qwen3-VL-30B			GPT-5.2			Gemini-2.5-Pro		
	Acc.	TNR	TPR	Acc.	TNR	TPR	Acc.	TNR	TPR	Acc.	TNR	TPR	Acc.	TNR	TPR	Acc.	TNR	TPR
Photo	57.41	100.00	14.82	83.73	100.00	67.45	52.09	100.00	4.18	82.14	100.00	64.27	98.91	99.95	97.86	94.70	100.00	89.41
Art Painting	54.70	100.00	9.41	79.55	100.00	59.09	52.91	100.00	5.82	77.23	100.00	54.45	99.02	100.00	98.05	95.80	100.00	91.59
Cartoon	55.23	100.00	10.45	81.89	100.00	63.77	52.80	100.00	5.59	82.50	100.00	65.00	97.95	100.00	95.91	93.23	100.00	86.45
Sketch	53.36	100.00	6.73	73.07	100.00	46.14	52.66	100.00	5.32	76.00	100.00	52.00	95.61	99.64	91.59	90.30	99.86	80.73
Random guess	50.00	50.00	50.00	50.00	50.00	50.00	50.00	50.00	50.00	50.00	50.00	50.00	50.00	50.00	50.00	50.00	50.00	50.00

Table 13: **Rotation recognition performance across PACS domains (10° – 90°).** Best and worst accuracy per model across domains are highlighted in teal and red, respectively. Performance aggregated over rotations from 10° to 90° in increments of 10°. While TNR remains near-perfect across all models, TPR varies significantly across domains, with strong performance on photographs and substantial degradation on sketches, indicating limited geometric robustness.

### I.3 PACS identity experiment results

Domain	Qwen2.5-VL-7B			Qwen2.5-VL-32B			Qwen3-VL-8B			Qwen3-VL-30B			GPT-5.2			Gemini-2.5-Pro		
	Acc.	TNR	TPR	Acc.	TNR	TPR	Acc.	TNR	TPR	Acc.	TNR	TPR	Acc.	TNR	TPR	Acc.	TNR	TPR
Photo	53.50	100.00	7.00	100.00	100.00	100.00	100.00	100.00	100.00	100.00	100.00	100.00	100.00	100.00	100.00	100.00	100.00	100.00
Art Painting	52.75	100.00	5.50	100.00	100.00	100.00	100.00	100.00	100.00	100.00	100.00	100.00	100.00	100.00	100.00	100.00	100.00	100.00
Cartoon	76.75	100.00	53.50	100.00	100.00	100.00	100.00	100.00	100.00	100.00	100.00	100.00	99.75	100.00	99.50	100.00	100.00	100.00
Sketch	92.25	100.00	84.50	100.00	100.00	100.00	100.00	100.00	100.00	99.75	100.00	99.50	100.00	100.00	100.00	100.00	100.00	100.00
Random guess	50.00	50.00	50.00	50.00	50.00	50.00	50.00	50.00	50.00	50.00	50.00	50.00	50.00	50.00	50.00	50.00	50.00	50.00

Table 14: **Model performance for the identity transformation on PACS.** Best accuracy values per model across domains are highlighted in teal, including ties, while worst values are shown in red. All models achieve near-perfect performance across domains, except Qwen2.5-VL-7B, which shows lower TPR on Photo and Art despite perfect TNR.

## I.4 Model performance with In-Context Learning

ICL Setting	Qwen2.5-VL-7B		Qwen2.5-VL-32B		Qwen3-VL-8B		Qwen3-VL-30B		GPT-5.2		Gemini-2.5-Pro	
	TNR	TPR	TNR	TPR	TNR	TPR	TNR	TPR	TNR	TPR	TNR	TPR
None	100.00	00.00	97.87	06.38	100.00	00.00	100.00	02.13	93.62	34.04	100.00	38.30
Few-shot	100.00	00.00	65.96	51.06↑	100.00	34.04↑	78.72	72.34↑	91.49	85.11↑	97.87	34.04↓
Rotational Grid	100.00	00.00	91.49	12.77↑	65.96	65.96↑	23.40	87.23↑	72.34	97.87↑	93.62	48.94↑

(a) Malayalam (top-tier script)

ICL Setting	Qwen2.5-VL-7B		Qwen2.5-VL-32B		Qwen3-VL-8B		Qwen3-VL-30B		GPT-5.2		Gemini-2.5-Pro	
	TNR	TPR	TNR	TPR	TNR	TPR	TNR	TPR	TNR	TPR	TNR	TPR
None	100.00	00.00	100.00	13.95	100.00	00.00	100.00	00.00	88.37	37.21	97.67	51.16
Few-shot	100.00	00.00	67.44	58.14↑	97.67	09.30↑	76.74	67.44↑	74.42	86.05↑	83.72	34.88↓
Rotational Grid	100.00	00.00	93.02	09.30↓	81.40	60.47↑	34.88	88.37↑	53.49	90.70↑	83.72	39.53↓

(b) Grantha (top-tier script)

ICL Setting	Qwen2.5-VL-7B		Qwen2.5-VL-32B		Qwen3-VL-8B		Qwen3-VL-30B		GPT-5.2		Gemini-2.5-Pro	
	TNR	TPR	TNR	TPR	TNR	TPR	TNR	TPR	TNR	TPR	TNR	TPR
None	100.00	00.00	88.00	16.00	100.00	00.00	100.00	00.00	100.00	20.00	96.00	32.00
Few-shot	100.00	00.00	68.00	76.00↑	100.00	16.00↑	68.00	72.00↑	80.00	68.00↑	92.00	32.00
Rotational Grid	100.00	00.00	88.00	24.00↑	72.00	88.00↑	40.00	76.00↑	60.00	88.00↑	88.00	56.00↑

(c) Tengwar (medium-tier script)

ICL Setting	Qwen2.5-VL-7B		Qwen2.5-VL-32B		Qwen3-VL-8B		Qwen3-VL-30B		GPT-5.2		Gemini-2.5-Pro	
	TNR	TPR	TNR	TPR	TNR	TPR	TNR	TPR	TNR	TPR	TNR	TPR
None	95.83	00.00	91.67	16.67	100.00	00.00	100.00	00.00	87.50	29.17	100.00	20.83
Few-shot	100.00	00.00	58.33	45.83↑	100.00	12.50↑	50.00	95.83↑	83.33	66.67↑	91.67	25.00↑
Rotational Grid	100.00	00.00	100.00	20.83↑	33.33	83.33↑	04.17	100.00↑	54.17	87.50↑	83.33	58.33↑

(d) Balinese (medium-tier script)

ICL Setting	Qwen2.5-VL-7B		Qwen2.5-VL-32B		Qwen3-VL-8B		Qwen3-VL-30B		GPT-5.2		Gemini-2.5-Pro	
	TNR	TPR	TNR	TPR	TNR	TPR	TNR	TPR	TNR	TPR	TNR	TPR
None	100.00	00.00	65.38	15.38	100.00	00.00	100.00	03.85	100.00	07.69	100.00	50.00
Few-shot	100.00	00.00	88.46	19.23↑	100.00	11.54↑	92.31	50.00↑	92.31	73.08↑	96.15	26.92↓
Rotational Grid	100.00	00.00	100.00	00.00↓	100.00	11.54↑	73.08	50.00↑	69.23	65.38↑	100.00	46.15↓

(e) Braille (low-tier script)

ICL Setting	Qwen2.5-VL-7B		Qwen2.5-VL-32B		Qwen3-VL-8B		Qwen3-VL-30B		GPT-5.2		Gemini-2.5-Pro	
	TNR	TPR	TNR	TPR	TNR	TPR	TNR	TPR	TNR	TPR	TNR	TPR
None	100.00	00.00	100.00	31.03	100.00	03.45	100.00	00.00	96.55	27.59	100.00	51.72
Few-shot	100.00	03.45↑	72.41	89.66↑	100.00	41.38↑	100.00	62.07↑	100.00	86.21↑	100.00	27.59↓
Rotational Grid	100.00	00.00	100.00	31.03	86.21	86.21↑	75.86	75.86↑	86.21	96.55↑	93.10	72.41↑

(f) Anglo-Saxon Futhorc (low-tier script)

Table 15: Model performance with In-Context Learning